

NEW HIGH-PERFORMING CERAMIC TILE COMPOSITIONS

J. García-Ten⁽¹⁾, A. Moreno⁽¹⁾, M.F. Quereda⁽¹⁾, A. Saburit⁽¹⁾
J. García-Sainz⁽²⁾, J. Manrique⁽²⁾, J. Usó⁽²⁾

⁽¹⁾Instituto de Tecnología Cerámica-
Asociación de Investigación de las Industrias Cerámicas.
Universitat Jaume I. Castellón. Spain

⁽²⁾FERRO SPAIN, S.A. Almazora (Castellón). Spain.

ABSTRACT

The present study was undertaken to determine the feasibility of fabricating ceramic tiles with compositions having a high alumina content (40%), with a view to substantially improving the mechanical properties of current ceramic tiles. These tiles must be made at existing facilities, so that tile behaviour throughout the manufacturing process should not excessively modify process variables. In this respect, one of the possible disadvantages stems from the high refractoriness of alumina. Different fluxes have therefore been studied that enable obtaining very low water absorption (<0.1%) at temperatures approaching 1200°C.

It has been observed that the use of mixtures of nepheline and spodumene enables producing pieces with zero apparent porosity at temperatures close to 1200C. However, closed porosity and pore size in the tiles are high, which adversely affect polished tile stain resistance.

It has been verified that pore size decreases as alumina particle size becomes smaller, although total porosity does not change significantly. This is because alumina particles form a "skeleton" that prevents the advance of the sintering process.

Reducing the alumina content allows making tiles with levels of closed porosity similar to those of polished porcelain tile. The admissible maximum alumina content that provides tiles with an appropriate level of closed porosity was found to lie between 30 and 35%, depending on alumina particle size.

Finally, one of these compositions has been characterised. This composition significantly improved tile aesthetic properties (whiteness and gloss) and mechanical properties (scratch and wear resistance).

1. INTRODUCTION

One of the present tendencies in the ceramic industry is to attempt to extend the fields of use of ceramic tiles, since current market levels of these products have stabilised. In some cases, this is done by engineering enhanced technical and/or aesthetic performance features with regard to already existing qualities.

Porcelain tile is currently the traditional ceramic product with the best technical performance^[1-2], although in view of the raw materials mainly used in manufacturing this material (clays, feldspars and quartz), it is difficult to improve porcelain tile properties.

Alumina currently finds limited use in the manufacture of traditional ceramic bodies, only tending to be used as an opacifier in some porcelain tile compositions^[3]. However, alumina is widely used in other ceramic products because of its high hardness and wear resistance, and the absence of phase transformations during firing, which provides it with high resistance to thermal shock^[4-5].

These benefits have already been used in the manufacture of electric porcelain, where alumina has progressively replaced quartz to improve the mechanical and electrical properties of these products^[6-7]. This improvement stems from the elimination of microcracks that arise during cooling as a result of the mismatch between the thermal expansion of quartz particles and the glassy matrix that surrounds them. The smaller coefficient of expansion of alumina reduces the arising stresses and therefore, the generation of such defects^[8].

The present study has been undertaken to determine the feasibility of making polished ceramic tiles with compositions having a high alumina content, in order to substantially improve mechanical properties compared with current ones. These tiles need to be fabricated at present facilities, so that their behaviour throughout the manufacturing process should not require modifying operating variables excessively. One of the constraints that needs to be addressed is related to the firing cycles, especially regarding the peak temperature at which these compositions are to be processed to achieve the required final properties.

2. EXPERIMENTAL

In performing the work, compositions have been prepared of which a series of properties has been determined, such as fusibility, porosity, microstructure, mechanical and aesthetic properties, etc. The procedures used for preparing these compositions, forming, firing and testing the pieces are briefly described below.

Preparation of the compositions

All the compositions were prepared by wet milling in planetary ball mills for the time required to achieve a 1% reject on a 40 μ m sieve. The resulting suspensions were dried under infrared lamps.

Forming and firing of test specimens

Test specimens, 6mm thick and of 40mm diameter, were formed by uniaxial pressing at a pressure of 400kg/cm². After drying in an oven at 110°C, the specimens

were fired in an electric laboratory kiln at different peak temperatures with a 6-min dwell time. The heating rate was 25°C/min and cooling was by forced convection.

Linear shrinkage (LS), bulk density (D_{ap}) and water absorption (WA)^[9] of the fired test specimens were determined. These values were used to calculate total porosity (ϵ_T), apparent porosity (ϵ_A), and closed porosity (ϵ_C) from the following equations:

$$\epsilon_T = \left(1 - \frac{D_{ap}}{D_R}\right) 100 \quad \epsilon_A = WA \cdot D_{ap} \quad \epsilon_C = \epsilon_T - \epsilon_A$$

where D_R is true density of each composition at the temperature that provides minimum total porosity (T_M).

Observation of microstructure

Specimen microstructure was observed by optical microscopy using the bright field signal. For this, test specimens were fired at T_M , and then polished with progressively finer grain size abrasive, first with silicon carbide and subsequently with diamond up to abrasive with a mean grain size of 1 μ m. Some of the specimens were also observed by scanning electron microscopy using the backscattered electron signal, in which the changes in the level of greys are associated with compositional changes.

Aesthetic properties

- **Chromatic co-ordinates.** The chromatic co-ordinates (L^* , a^* , b^*) were determined in a diffuse reflectance spectrophotometer using a D65 type illuminant and standard observer at 10°.
- **Stain resistance.** First, the chromatic co-ordinates of the polished test specimens were measured (L_0^* , a_0^* and b_0^*). The specimen surface was then impregnated with an indelible ink labeller and left to dry for some minutes, after which the ink rests were wiped off with a water-dampened cloth. After drying the surface with a dry cloth, the chromatic co-ordinates were measured again and the change in colour was calculated by means of parameter ΔE^* from the equation:

$$\Delta E^* = \sqrt{(L^* - L_0^*)^2 + (a^* - a_0^*)^2 + (b^* - b_0^*)^2}$$

This parameter is termed ΔE_0^* . The test specimens were then subjected to periodic cleaning stages by means of a device that applied a cloth soaked in ethanol, which rotated at a constant rate, with a set load on the surface. After each cleaning stage, the chromatic co-ordinates of the surface were measured again, then calculating parameter ΔE^* , which indicated the colour change in the test specimen. This process was repeated until test specimen colour remained constant (ΔE_F^*).

Mechanical properties

- **Determination of the critical scratch load (L_C).** The test was conducted with a nanoindentation apparatus fitted with a diamond indenter of conical

geometry (Rockwell) with a spherical tip of 25 μm radius. Scratches, 1mm long, were made by progressively increasing the load, from 0 to 2000 mN. Before and after surface scratching, the stylus travelled across the test zone applying a minimum load, thus recording the original and final surface profile. This enabled detecting changes in depth of the scratched region. After the scratch test, topographic maps were obtained with the optical profilometer for visual observation of the changes in the scratching mechanism.

- **Loss of gloss during wear.** The test was performed with a modified PEI type abrasion tester to reduce the surface area of the abraded circle. The test consists of determining the evolution of gloss after performing abrasion stages of 5000 revolutions. Gloss measurements were made with a reflectometer at a 60° angle of incidence.
- **Determination of the rate of wear.** The wear tests were carried out in a tribometer with the pin on disk arrangement (Figure 1). SiC abrasive disks (grit 180) were placed under the pin that was applied with a load of 1N. The test specimens were subjected to successive polishing stages, and weighed before and after each test stage. At the end of the test, specimen weight loss was plotted versus test duration, expressed in number of revolutions. These experimental points, which fit a straight line, were used to calculate the slope whose value is the rate of wear of the tested piece.

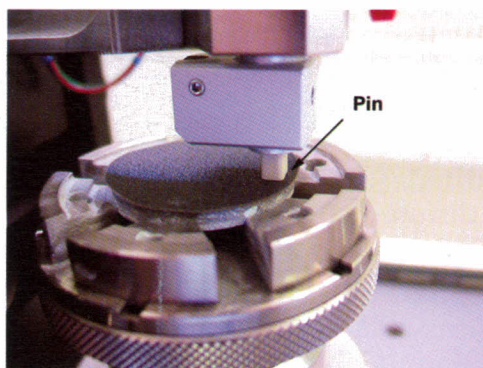


Figure 1. Pin on disk arrangement in the tribometer

3. SELECTION OF THE FLUXING SYSTEM

The following materials were studied as high-temperature fluxes:

- Frits
- Feldspars (sodium and potassium)
- Feldspathoids (nepheline)
- Pyroxenes (spodumene)

3.1. FRITS

3.1.1 Experimental

The alumina used in the study was a calcined alumina with a mean particle size of 4.3 μm . All the frits used were commercial frits of the following types:

- Transparent single-fire frit (FC)
- Opaque single-fire frit (FO)
- Fluxing alkaline frit (FFA)
- Fluxing boron frit (FFB)

The studied compositions are listed in Table 1. The alumina content was kept constant in all the frits, modifying the type of frit.

| Composition | AFC | AFO | AFFA | AFFB |
|----------------|-----|-----|------|------|
| Alumina | 45 | 45 | 45 | 45 |
| FC | 55 | - | - | - |
| FO | - | 55 | - | - |
| FFA | - | - | 55 | - |
| FFB | - | - | - | 55 |

Table 1. Formulated compositions (wt%).

3.1.2. Results

All the tested compositions yielded pieces with a reduced dry bulk density value (1.50g/cm^3). As it is known that the presence of alumina appreciably increases the true density of the compositions, the initial porosity of the pieces can be estimated around 50%. This will therefore involve high shrinkage during firing.

Figure 2 shows the vitrification diagrams of compositions AFC and AFO. These diagrams show that using these types of frits (FC and FO) does not allow obtaining low values of apparent porosity or total porosity in the tested range of temperatures (1200-1260°C). This indicates that the pieces have a very porous structure, which almost exclusively consists of apparent porosity in which the pores are interconnected.

In order to determine why closed porosity of the pieces could not be reduced, we analysed the crystalline species present in composition AFC, fired at 1260°C. Figure 3 shows the corresponding diffractogram, in which the presence of a series of peaks can be observed, corresponding to the following crystalline species: corundum, anorthite and gahnite. The first of these is attributable to the alumina addition, whereas the last two have crystallised during firing as a result of the presence of alkaline-earth oxides (from the frit) and alumina (from the frit and partial dissolution of alumina). The presence of these crystals, in important amounts to judge by their peak areas, notably increases the viscosity of the liquid phase that surrounds the alumina particles, preventing the pieces from sintering at the tested temperatures.

It was therefore decided to test fluxing alkaline and boron frits, which were both free of alkaline-earth oxides. Figures 2 and 4 depict their vitrification diagrams. Frit FFA is observed to provide smaller total and apparent porosity values, although at the maximum temperature tested (1260°C), apparent porosity cannot be eliminated ($\epsilon_A=12\%$). In contrast, frit FFB (Figure 4) vitrifies ($\epsilon_A=0$) the pieces at very low temperatures, of the order of 875°C. However, the value of total porosity is high,

which indicates the presence of a high proportion of closed porosity in the pieces. This was confirmed after polishing and observation by optical microscopy (Figure 5).

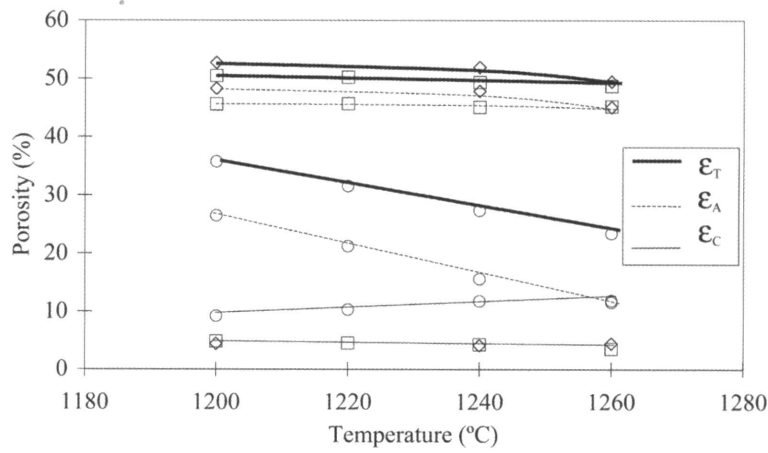


Figure 2. Evolution of ϵ_T , ϵ_A and ϵ_C with temperature for compositions AFC(\diamond), AFO(\square) and AFFA(O).

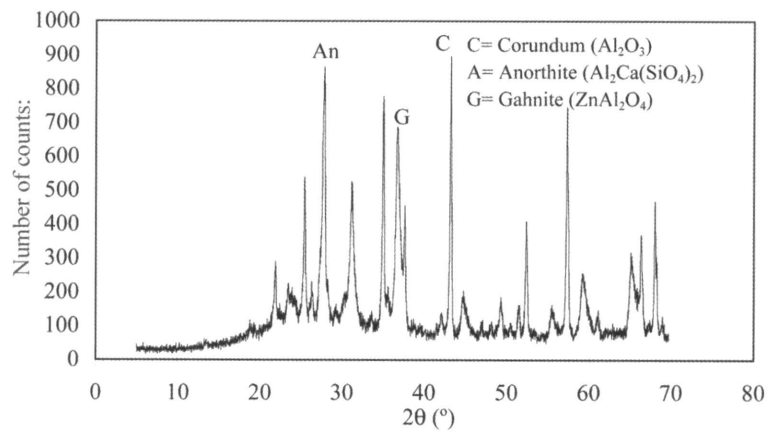


Figure 3. X-ray diffraction of composition AFC fired at 1260°C.

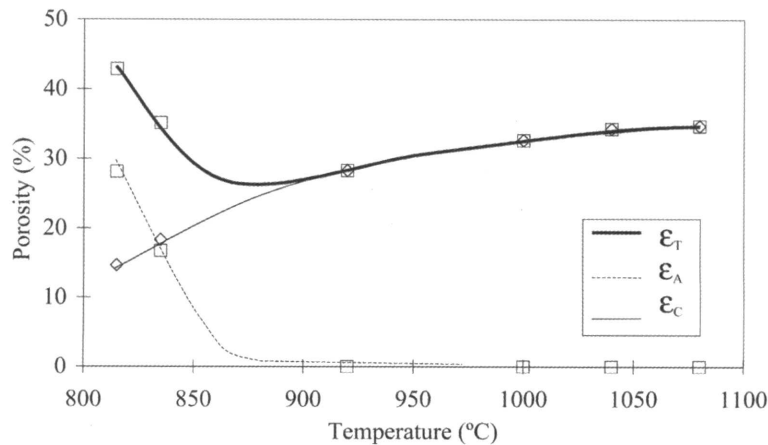


Figure 4. Evolution of ϵ_T , ϵ_A and ϵ_C with temperature for composition AFFB.

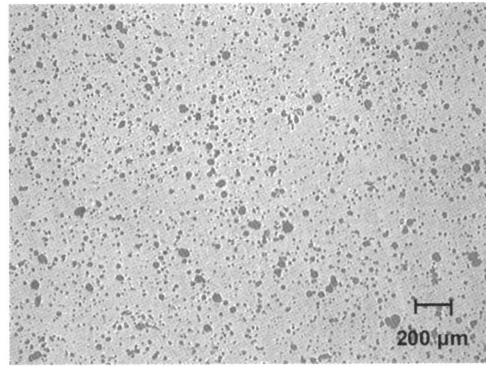


Figure 5. Microstructure of piece AFFB at 900°C.

In order to improve the characteristics of the pieces obtained with frit FFB, compositions with smaller frit contents were tested. Figure 6 shows the evolution of apparent, total and closed porosity of the pieces with frit content. It can be observed that whereas reducing the frit content from 55 to 50% does not significantly modify the properties of the resulting pieces, when this is reduced below 50%, apparent porosity and total porosity increase sharply. This indicates that, although the use of fluxing boron frits provides the pieces with zero apparent porosity, closed porosity remains very high (30%) compared with that of porcelain tile (8-10%), which advises against polishing these pieces because of their great stain retention capacity.

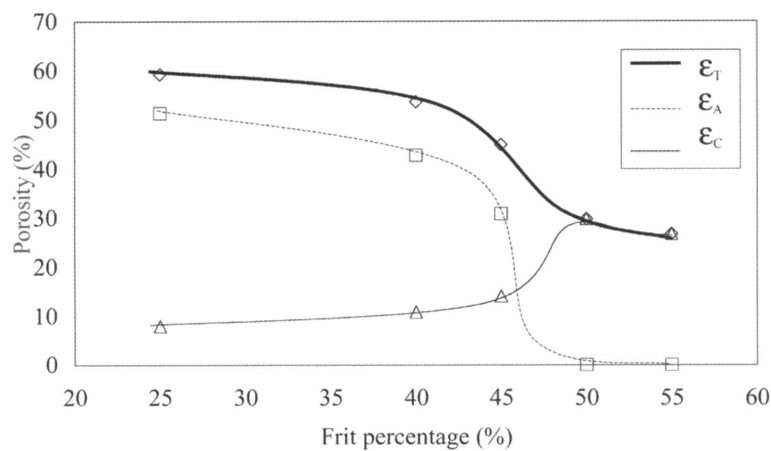


Figure 6. Evolution of ϵ_T , ϵ_A and ϵ_C with frit FFB content.

3.2 NATURAL RAW MATERIALS

3.2.1. Experimental

The natural raw materials used in this part of the work were as follows:

- Potassium feldspar (65% orthoclase)
- Sodium feldspar (85% albite)
- Nepheline syenite (30% nepheline + 50% orthoclase)
- Spodumene (75% spodumene)

The studied compositions are detailed in Table 2. The alumina content was kept constant in all of these compositions, modifying the type of raw material flux to be studied.

| Composition | AK | ANa | AN | AE |
|--------------------|----|-----|----|----|
| Alumina | 45 | 45 | 45 | 45 |
| Potassium feldspar | 55 | - | - | - |
| Sodium feldspar | - | 55 | - | - |
| Nepheline | - | - | 55 | - |
| Spodumene | - | - | - | 55 |

Table 2. Formulated compositions (wt%).

3.2.2. Results

The vitrification diagrams of these compositions are shown in Figure 7. It can be observed that none of the tested raw materials, alone, enable obtaining pieces free of apparent porosity at temperatures close to 1200°C. However, some of these raw materials are more effective than others in reducing porosity. Thus, whereas the variation of porosity with temperature of the pieces made with the compositions that contain potassium feldspar and spodumene is very low, the use of sodium feldspar, and especially of nepheline, provides a more pronounced variation in porosity, yielding practically zero values for apparent porosity at 1280°C when nepheline is used.

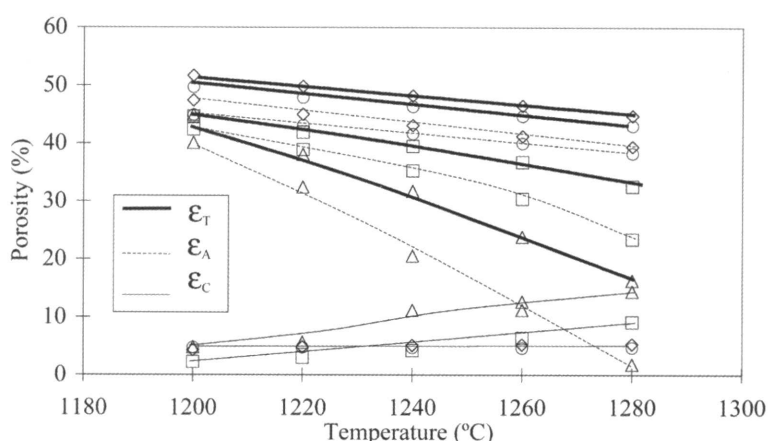


Figure 7. Evolution of ϵ_T , ϵ_A and ϵ_C with temperature for compositions AK(\diamond), ANa(\square), AN(Δ) and AE(O).

The different behaviour of these raw materials during firing is to be explained by the melting temperature of these minerals, since the existence of eutectic points of importance between each of these raw materials and alumina have not been reported in the literature. Thus, orthoclase and spodumene display high melting points, 1530°C and 1455°C respectively, whereas albite and nepheline melt at much lower temperatures, 1118°C and 1020°C respectively^[10].

Based on these results, nepheline was selected to further pursue the study. With a view to reducing vitrification temperature, T_V ($\epsilon_A = 0$), of this composition, it was decided to use mixtures of raw materials that provided eutectic points at moderate temperatures. Mixtures were therefore tested of nepheline-spodumene and nepheline-wollastonite. These raw materials were selected because of the existence of eutectic points between Na_2O and K_2O of nepheline with Li_2O and CaO of spodumene and wollastonite respectively^[10]. The tested compositions are listed in Table 3.

| Composition | AN | ANE | ANE2 | ANW |
|--------------|----|-----|------|-----|
| Alumina | 45 | 45 | 45 | 45 |
| Nepheline | 55 | 45 | 35 | 45 |
| Spodumene | - | 10 | 20 | - |
| Wollastonite | - | - | - | 10 |

Table 3. Formulated compositions (wt%).

Figure 8 plots the vitrification diagrams of these compositions. Observation of these diagrams reveals that the use of nepheline-spodumene mixtures increases the rate at which the pieces vitrify, providing very low apparent porosity values at noticeably lower temperatures. With respect to spodumene, it can be observed that in the tested range, the larger the spodumene content in the mixture, the lower is the vitrification temperature. In contrast, the use of the nepheline-wollastonite mixtures is ineffective in the tested percentage compared with the use of nepheline.

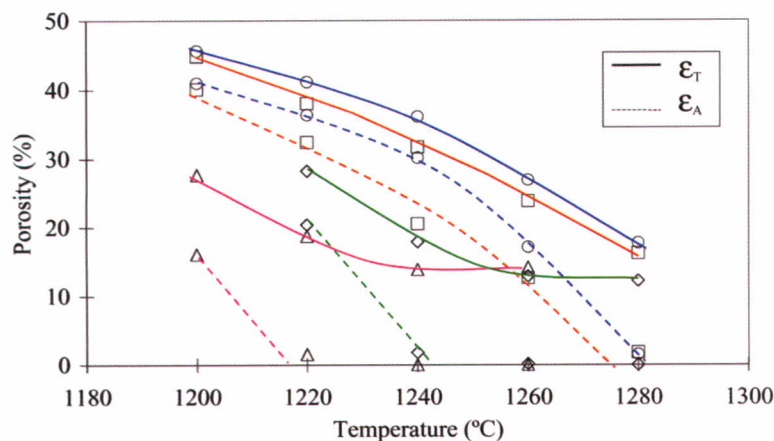


Figure 8. Evolution of ϵ_T , ϵ_A and ϵ_c with temperature for compositions AN(\square), ANE(\diamond), ANE2(Δ) and ANW(\circ).

When compositions were available that enabled obtaining pieces with zero apparent porosity at temperatures close to 1200°C , the resulting test specimens that had reached the maximum densification state were polished and observed by optical microscopy. Although it was already known that all these compositions displayed a greater closed porosity than porcelain tile compositions, these tests were run to determine the size and morphology of the pores present. Figure 9 shows the appearance of these pieces, together with a polished porcelain tile prepared under the same conditions for comparative purposes.

These micrographs show that the formulated compositions display greater porosity than porcelain tile, and a totally different porous structure. Thus, whereas porcelain tile mainly contains small, irregularly shaped pores, the test pieces have appreciably larger size pores, which are more rounded. This indicates the presence of a large amount of low viscosity liquid phase in the final sintering stages^[11]. On the other hand, the pore size of the composition with wollastonite is appreciably larger than that of the compositions with spodumene.

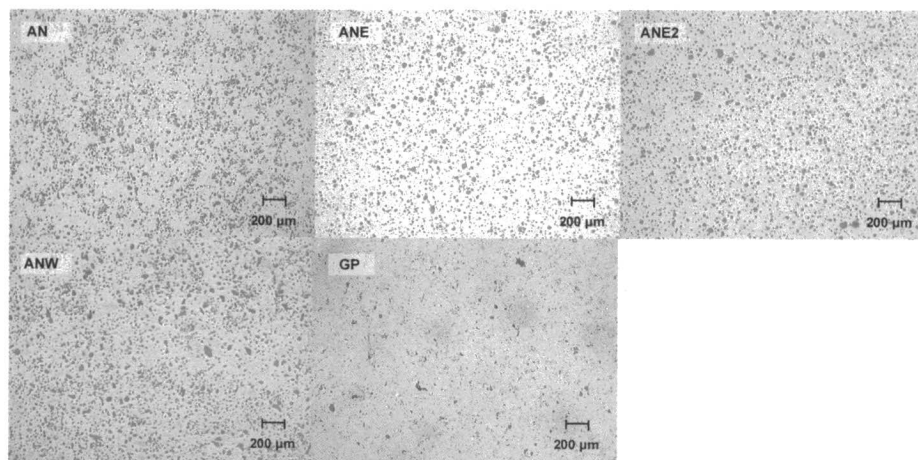


Figure 9. Microstructure of test pieces AN, ANE, ANE2, ANW and GP fired at T_M .

3.2.3. Mechanical properties of composition ANE2

Of the compositions studied up to this point, the one that exhibited the smallest closed porosity, as well as a firing temperature closest to 1200°C was ANE2. Although this composition produced pieces with a more porous microstructure than porcelain tile, it was considered of interest to determine certain mechanical properties (scratch and wear resistance) with a view to establishing whether the presence of alumina contributed better mechanical properties to the pieces.

Figure 10 plots the mass loss of the test piece made with composition ANE2 during wear. For comparative purposes, it also includes the results of a porcelain tile composition (GP). It can be observed that in both cases a straight line is obtained whose slope indicates the rate of mass loss during the test. The slope corresponding to ANE2 is notably lower than that of GP, demonstrating the effectiveness of alumina in raising tile wear resistance.

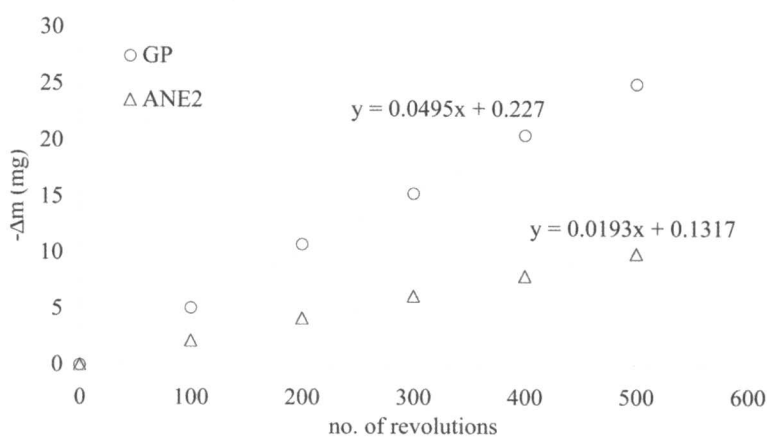


Figure 10. Wear resistance of composition ANE2.

The scratch resistance tests are depicted in Figure 11. The background of the graph displays the topographic map of the test pieces, showing the evolution of the tracks produced on raising the load applied by the indenter. The lines plotted correspond to two profiles of the specimen surface: first on the original surface and second after applying the load.

In this case as well, significant differences are noticeable between the porcelain tile and composition ANE2. The topographies show that the scratch made on the porcelain tile surface produces flaking at much lower loads ($L_c=700\text{mN}$) than on ANE2. In the latter, although tracks also start appearing at low load values, flaking first occurs at considerably higher loads ($L_c=1500\text{mN}$). With regard to the profiles of the original pieces, the profile corresponding to ANE2 displays more peaks at lower loads as a result of the larger number and size of the pores in these pieces. However, the plot of the test shows that the ANE2 profile hardly departs from the original profile until high loads (1500mN) are applied, except at points where pores and breaks previously existed, albeit without causing great damage. In contrast, the GP profile changes abruptly at loads of 700mN , after which it exhibits pronounced swings. In this case, the peaks higher than the surface of the piece are the result of the presence of chips caused by surface flaking, detected by the stylus and mapped.

Summing up, it may be concluded that although the presence of greater porosity in composition ANE2 favours scratching of the piece, because the pores act as anchoring points for the indenter, the presence of alumina provides the test pieces with better mechanical behaviour. These differences have been reported by other authors^[8] and are attributed to the presence of microcracks caused by the mismatch between the coefficients of expansion of the quartz crystals and the surrounding glassy matrix, an effect that does not arise in the alumina compositions.

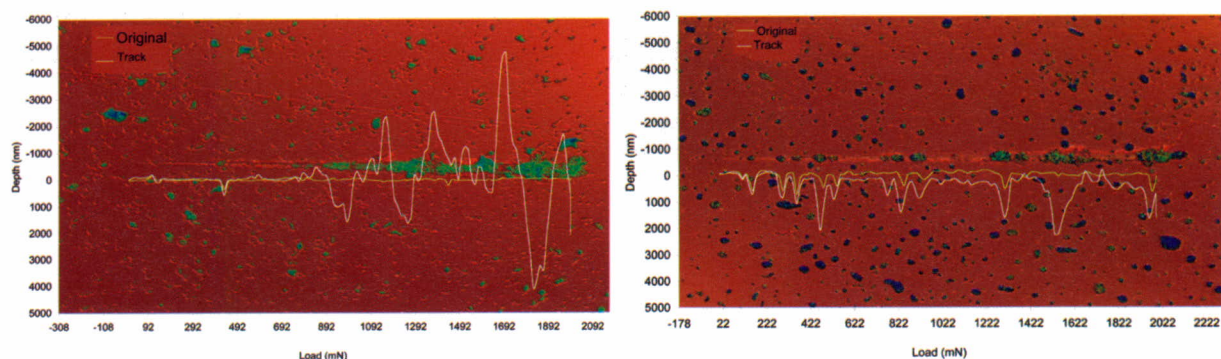


Figure 11. Scratch resistance of GP (left) and ANE2 (right).

4. IMPROVEMENT OF TILE MICROSTRUCTURE

After studying and selecting the most appropriate fluxing mixture to process these compositions at temperatures close to 1200°C , and verifying that their scratch and wear resistance was notably superior to that of the polished porcelain tile specimens, the next phase of the study was undertaken. This consisted of improving tile microstructure. This part of the work had a twofold objective, namely to reduce the closed porosity of the pieces and to obtain a pore system of smaller-size pores. This would improve tile mechanical properties and assure scarce stain retention after the polishing stage. For this, alumina particle size and content in the composition were modified.

4.1 INFLUENCE OF ALUMINA PARTICLE SIZE

4.1.1. Experimental

Figure 12 plots the particle-size distribution of the three tested aluminas. Sample A corresponds to the alumina used in the previous stages of the study.

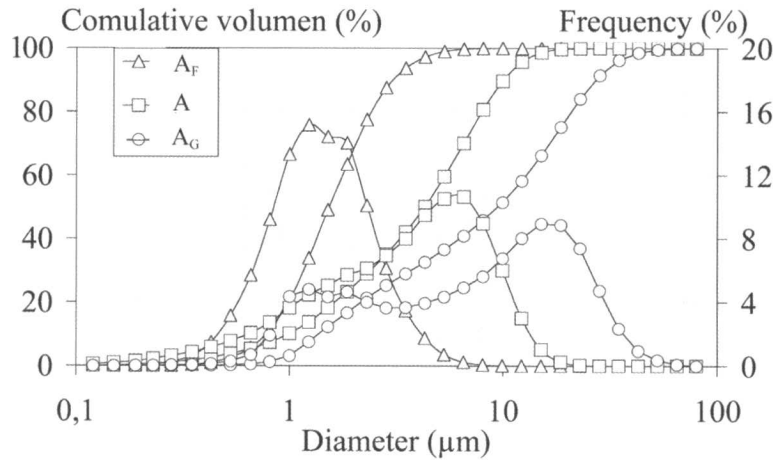


Figure 12. Alumina particle-size distribution.

4.1.2. Results

Figure 13 plots the variation of T_V and T_M , as well as total porosity at T_M (equal to closed porosity, as apparent porosity is zero in these compositions at T_M), with mean particle size (d_{50}) of the alumina addition. It shows that reducing alumina particle size also lowers both T_V and T_M , indicating a rise in the vitrification rate. This effect must be attributed to the influence that alumina particle size has on green tile microstructure. Thus, as alumina particle size decreases, pore-size distribution shifts towards smaller sizes. This microstructural difference and the fact that smaller size pores are eliminated as firing temperature increases, while intermediate and large-size pores grow, lead to the greater sintering rate of composition A^{FNE2}[12-13]. The reduction in porosity of the pieces is in accordance with this sintering mechanism.

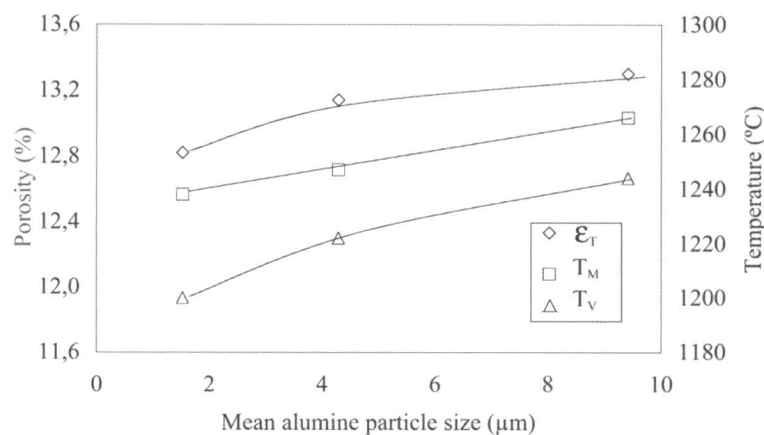


Figure 13. Evolution of T_V , T_M and ϵ_T with d_{50} .

Next, in order to determine the effect of alumina particle size on the microstructure of the pieces, these were polished and observed by optical microscopy. Figure 14 shows the appearance of the pieces fired at T_M . It can be observed that as alumina particle size decreases, microstructure evolves towards a porous system made up of smaller size pores, although the pores are more numerous. However, even when using the smaller particle size alumina, such compact microstructures as those of the porcelain tile specimens are not obtained (please see Figure 9).

There could be two reasons for this resulting microstructure. On the one hand, it could be due to the rise in liquid-phase viscosity as a result of the partial dissolution of alumina, especially when the smaller particle size alumina is used. On the other, this could also be due to an excessive alumina content, whose particles could enter into contact with each other during the sintering process, forming a "skeleton" that arrests the sintering process.

When the crystalline species of the pieces corresponding to the three compositions were determined, no significant changes were found in the area corresponding to the corundum peak. This indicates that if the alumina did dissolve in any measure, this dissolution would be quite minor. For this reason, these pieces were then examined by SEM. Figure 15 shows the appearance of the pieces, in which the alumina particles display a clearer colour than the surrounding glassy phase. The alumina particles exhibit well-defined edges, which is consistent with the foregoing results and confirms that these particles do not dissolve in firing. Furthermore, independently of their size, the alumina particles display numerous interparticle contacts, forming a "skeleton" that arrests the sintering process. The formation of this skeleton has been observed by other authors, who indicate that pieces cannot be obtained at 100% relative density ($\epsilon_T=0$) when the alumina content exceeds 15% by volume^[14].

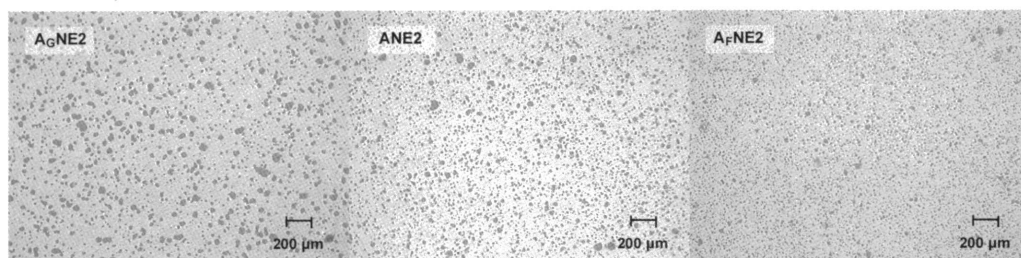


Figure 14. Microstructure of test pieces A_GNE2 , $ANE2$ and A_FNE2 fired at T_M .

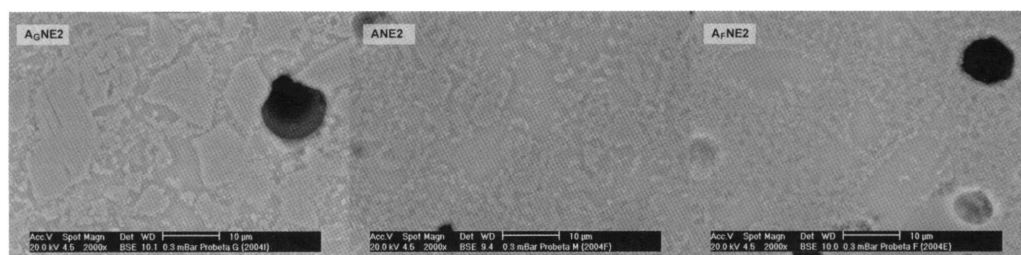


Figure 15. Micrographs of compositions A_GNE2 , $ANE2$ and A_FNE2 fired at T_M .

4.2 INFLUENCE OF ALUMINA CONTENT

4.2.1. Experimental

The studied compositions are set out in Table 4. In these compositions, the alumina content has been progressively reduced and that of the nepheline-spodumene mixture increased, holding the nepheline-to-spodumene proportion.

| Composition | A20NE2 | A30NE2 | A40NE2 | A45NE2 |
|------------------|--------|--------|--------|--------|
| Alumina A | 20 | 30 | 40 | 45 |
| Nepheline | 51 | 45 | 38 | 35 |
| Spodumene | 29 | 25 | 22 | 20 |

Table 4. Formulated compositions (wt%).

4.2.2. Results

The evolution of vitrification temperature, maximum densification, and total porosity ($\epsilon_T = \epsilon_C$, as $\epsilon_A = 0$ at T_M) with alumina are plotted in Figure 16. The reduction of alumina content produces a progressive reduction of T_v and T_M , as a result of the greater nepheline and spodumene content in the compositions. Furthermore, an important reduction is also detected in closed porosity, attaining similar values to those of porcelain tile (9-10%).

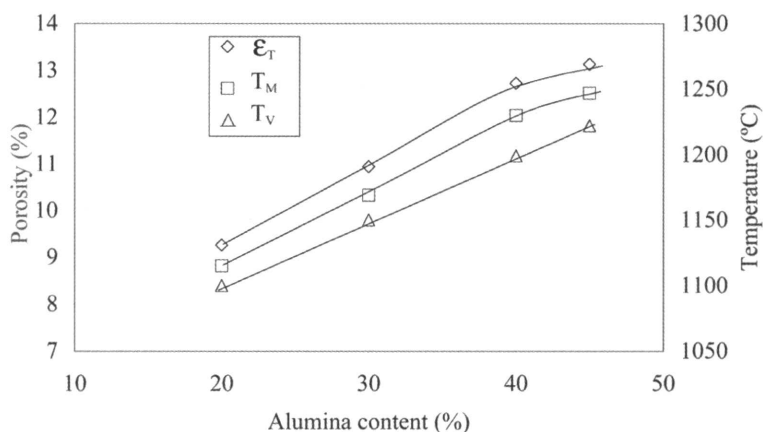


Figure 16. Evolution of T_v , T_M and ϵ_T with alumina content.

Figure 17 shows the appearance of the porous structure of the pieces examined by optical microscopy. It can be observed that as alumina content is reduced, porosity decreases, with a significant change being detected at alumina contents below 40%. Thus, higher alumina contents lead to excessively porous pieces, with many large rounded pores, whereas smaller amounts of alumina yield pieces with a less porous microstructure made up of smaller pores of more irregular shape, very similar to porcelain tile microstructure. These findings indicate that at alumina contents between 30% and 40%, contacts start to develop between the alumina particles that halt the sintering process.

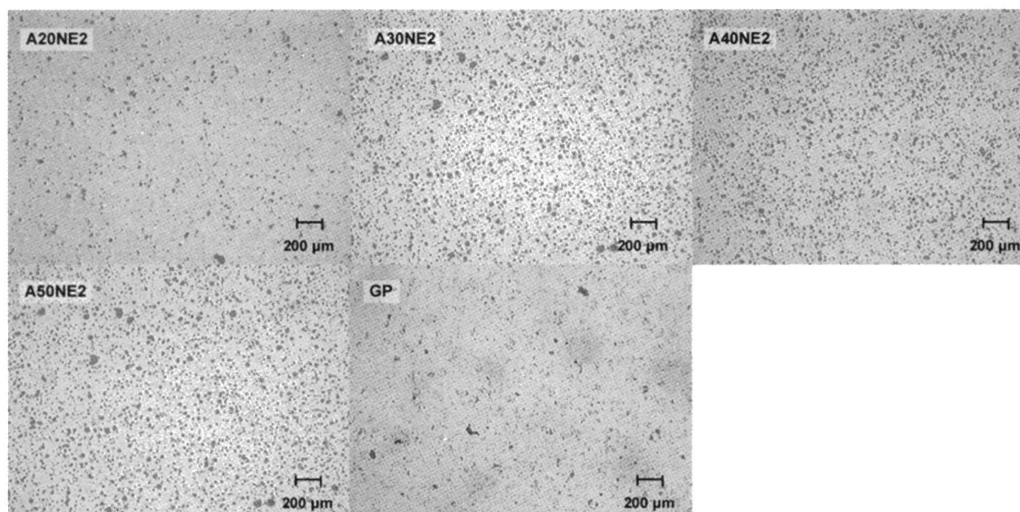


Figure 17. Microstructure of the pieces fired at T_M on modifying alumina content.

5. OPTIMISATION OF THE COMPOSITION

The previous sections confirmed that making pieces with an appropriate porous structure requires using small particle size alumina at contents below 40%. For this reason, in this phase of the work, compositions have been tested with A_F alumina contents of 30% and 35% (Table 5). Table 6 and Figure 18 present the values of T_V , T_M , ϵ_T , ϵ_A and ϵ_C , as well as the appearance of resulting specimen porous structure.

| Composition | A_F30NE2 | A_F35NE2 |
|---------------|------------|------------|
| Alumina A_F | 30 | 35 |
| Nepheline | 45 | 42 |
| Spodumene | 25 | 23 |

Table 5. Compositions formulated (wt%).

| Composition | A_F30NE2 | A_F35NE2 | GP |
|------------------|------------|------------|------|
| T_M (°C) | 1166 | 1189 | 1200 |
| T_V (°C) | 1142 | 1160 | 1190 |
| ϵ_T (%) | 10.6 | 11.6 | 9.6 |
| ϵ_A (%) | <0.1 | <0.1 | <0.1 |
| ϵ_C (%) | 10.6 | 11.6 | 9.6 |

Table 6. T_M , T_V , and properties at T_M of the compositions.

It can be observed that the compositions with alumina display slightly lower T_v and T_M values than the GP composition, particularly the composition with 30% alumina. This enables processing in industrial roller kilns. With regard to the values of porosity, it is to be noted that these compositions vitrify ($\epsilon_A=0$) at considerably lower temperatures than T_M , which assures zero apparent porosity in the maximum densification state. On the other hand, closed porosity values rise slightly with alumina content, which agrees with the observations made on studying the influence of alumina content (section 4.2). The microstructure obtained is very similar to that of composition GP, though closed porosity is slightly higher.

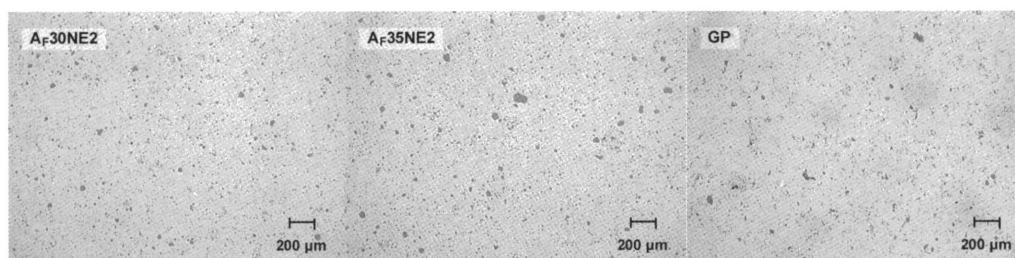


Figure 18. Microstructure of test pieces of compositions A_{F30NE2} and A_{F35NE2} fired at T_M .

As the alumina content in these compositions was lower than in the starting compositions, it was decided to run a series of tests to determine whether the performance of these compositions continued to be superior to those of porcelain tile. For this, the composition with 35% alumina was selected.

Table 7 lists the results obtained, which are compared with the usual range of values displayed by polished porcelain tile^[15].

| Properties | A_{F35NE2} | Porcelain tile |
|----------------|--------------|----------------|
| L_C (mN) | 1600 | 600-800 |
| W_P (mg/rev) | 0.024 | 0.045-0.060 |
| β_0 | 92.5 | 83-93 |
| β_F | 4.3 | 2.5-3.5 |
| no. rev | 3500 | 2300-2700 |
| L^* | 95 | 75-85 |
| a^* | 0.5 | 0-4 |
| b^* | 1.8 | 6-14 |
| ΔE_0^* | 8.8 | 6-15 |
| ΔE_F^* | 3.4 | 3-9 |

Table 7. Comparison of properties.

The presence of alumina is confirmed to notably increase the value of the critical load (L_c), yielding a value even higher than that of composition ANE2, probably due to lower porosity and smaller pore size. This means achieving low wear rate values (WP).

Gloss of the polished pieces (β_0) is in the high region of the range, because the greater refractive index of alumina counteracts the greater porosity of the pieces. On the other hand, composition A_F35NE2 exhibits a smaller loss of gloss during wear, as observed by the greater number of revolutions (no. rev.) required to stabilise final gloss (β_F).

The composition's degree of whiteness is very high as a result of the opacifying power of alumina and scarce colouring oxide content in the raw materials. Finally, stain resistance of the polished pieces is within the range of values provided by polished porcelain tile, shown by the ΔE_{0^*} values (initial stain retention) and ΔE_{F^*} values (irreversible stain retention).

6. CONCLUSIONS

The following conclusions may be drawn from the study:

1. The vitrification of compositions with a high alumina content at temperatures that allow processing these in current production facilities requires using vigorous fluxing systems. The study shows that the use of commercial frits of the crystalline, zirconium white and alkaline type does not allow vitrifying the pieces at 1200°C. On the other hand, the use of fluxing boron frits, which enable vitrification, produces excessive closed porosity.
2. Using nepheline-spodumene mixtures enables vitrifying these compositions, though this leads to pieces with larger porosity and pore size compared with those of polished porcelain tile.
3. Reducing alumina particle size leads to pieces with smaller pore size, although total porosity is not reduced significantly. This is due to the existence of numerous contact points between the alumina particles, which form a "skeleton" that arrests the sintering process.
4. When the alumina content in the composition is decreased, pieces can be fabricated with a porosity and pore size similar to those found in porcelain tile. The maximum alumina content for making ceramic tiles with an appropriate microstructure was found to lie between 30% and 35%, depending on alumina particle size.
5. A composition has been formulated with 35% alumina that enables making ceramic tiles with a microstructure similar to that of porcelain tile at temperatures slightly below 1200°C. This allows processing the composition in current industrial production facilities.
6. This ceramic tile composition substantially improves aesthetic properties (whiteness and gloss) and mechanical properties (scratch resistance and wear resistance) in respect of current polished porcelain tile properties, which opens up the possibility of extending the fields of use of this type of tile.

REFERENCES

- [1] BIFFI, G. Il gres porcellanato: manuale di fabbricazione e tecniche di impiego. Faenza: Faenza Editrice, 1997.
- [2] SÁNCHEZ, E. Technical considerations on porcelain tile products and their manufacturing process. In: Proceedings of the VII World Congress on Ceramic Tile Quality. Castellón. Cámara Oficial de Comercio, Industria y Navegación. Vol. I, Con 57-84, 2002.
- [3] BOSCARDIN, L.; KOCKEGEY LORENZ, R. Study on the use of alumina in fully vitrified stoneware mixtures. *Int. Ceram. J.*, 5, 13-17, 1995.
- [4] AUSTIN, C.R.; SCHOFIELD, H.Z; HALDY, N.L. Alumina in whiteware. *J. Am. Ceram. Soc.*, 29(12), 341-354, 1946.
- [5] GITZEN, W.H. (Ed.) Alumina as a ceramic material. Columbus: American Ceramic Society, 1970.
- [6] BLOOR, E.C. Electrical porcelain: a review. I. Production aspects. *J. Br. Ceram. Soc.*, 7(3), 77-84, 1970.
- [7] BLOOR, E.C. Electrical porcelain: a review. II. Technical aspects. *J. Br. Ceram. Soc.*, 7(5), 129-134, 1970.
- [8] WARSHAW, S.I.; SEIDER, R. Comparison of strength of triaxial porcelains containing alumina and silica. *J. Am. Ceram. Soc.*, 50(7), 337-343, 1967.
- [9] AMORÓS ALBARO, J.L. et al. Manual para el control de la calidad de materias primas arcillosas. Castellón: Instituto de Tecnología Cerámica, 1998.
- [10] LEVIN, E.M. et al. (Eds.) Phase diagrams for ceramists. Volume I. Columbus: The American Ceramic Society, 1985.
- [11] ORTS TARÍ, M. J. Sinterización de piezas de pavimento gresificado. Valencia: Universidad de Valencia, 1991. [PhD dissertation]
- [12] SACKS, M.D.; TSENG, T.-Y. Preparation of SiO₂ glass model powder compacts: Part 2, sintering. *J. Am. Ceram. Soc.*, 67(8), 532-537, 1984.
- [13] SACKS, M.D.; VORA, S.D. Preparation of SiO₂ glass model powder compacts: Part 3, enhanced densification by sol infiltration. *J. Am. Ceram. Soc.*, 71(4), 245-249, 1988.
- [14] BOCCACCINI, A.R. Glass matrix composite materials with dispersion reinforcement. A review. Part 1: historical development and fabrication techniques. *Verre*, 5 (2), 3-14, 1999.
- [15] SÁNCHEZ, E.; GARCÍA-TEN, J.; IBÁÑEZ, M.J.; FELÍU, C.; SÁNCHEZ, J.; SOLER, C.; SALES, J.; PORTOLÉS, J. Comparative study of polished porcelain tile properties. (Paper presented at Qualicer 2004)